Electronic Supplementary Material (ESI) for ChemComm.
This journal is © The Royal Society of Chemistry 2014

Supplementary Information

Real-time imaging and local elemental analysis of nanostructures in liquids

Edward A. Lewis,[a] Sarah J. Haigh,*[a] Thomas J. A. Slater,[a] Zheyang He,[a] Matthew A. Kulzick,[b] Mary G. Burke [a] and Nestor J. Zaluzec [a,*c]

[a] Materials Performance Centre and Electron Microscopy Centre, School of Materials, University of Manchester, Manchester, M13 9PL, UK

[b] BP Corporate Research Center, Naperville, Illinois USA

[c] Electron Microscopy Center, Argonne National Laboratory, Argonne, IL 60439, USA

Corresponding authors:

*Sarah Haigh: sarah.haigh@manchester.ac.uk

*Nestor Zaluzec: zaluzec@aaem.amc.anl.gov

Experimental Methods

E-cell assembly

The liquid e-cell used for this study was assembled using Protochips Poseidon E-chips and a modified Protochips Poseidon 200 Liquid Flow TEM Holder. The E-chips used were of a pair of 350 µm thick Si chips; within each chip was a lithographically fabricated 50 nm thick, 400 x 50 µm, electron transparent SiN_x window. Gold spacers deposited onto the corners of the bottom chips created a nominal vertical separation of 150 nm. The e-cell was almost completely filled with the aqueous nanoparticle "soup" solution, the balance of the volume being a small trapped pocket of air at atmospheric pressure. These air bubbles result in transient liquid-filled and liquid-depleted regions (Video S7).

Electron Microscopy

Imaging and XEDS analysis were carried out in a FEI Titan G2 80-200 S/TEM "ChemiSTEM™" instrument operated at 200 kV. Images were acquired in HAADF STEM mode with a probe current of 200 pA, a convergence semi-angle of 18.5 mrad and an inner collection semi-angle of 54 mrad. Spectrum images were acquired with two of the four SSD detectors turned on and the SiN_x window tilted toward these two detectors (Fig. S5).

STEM images were recorded using FEI TIA software and spectrum images were recorded using Bruker Esprit software. Post processing of XEDS data was carried out using Esprit software, for spectrum quantification (O_k/Si_k ratios) and line profiles Bremsstrahlung background subtraction was performed. 7 point averaging was applied to the line profiles presented in this work.

An FEI Tecnai G2 F30 microscope operated at 300 kV and equipped with a Gatan Imaging Filter spectrometer was used to record EELS spectra for the purpose of thickness (t/λ) measurements (Fig. S4). EELS spectra were recorded using Gatan Digital Micrograph software.

S1. Dry reference samples

A reference sample was prepared by drop casting the aqueous nanoparticle "soup" solution onto a 100 nm thick SiN_x window. Although this is thicker than is optimal for imaging, a 100 nm support thickness was chosen for comparison with the e-cell which has a total SiN_x window thickness of 100 nm (comprised of two 50 nm windows). Spectral images taken for the dry reference sample are shown in Fig. S1.

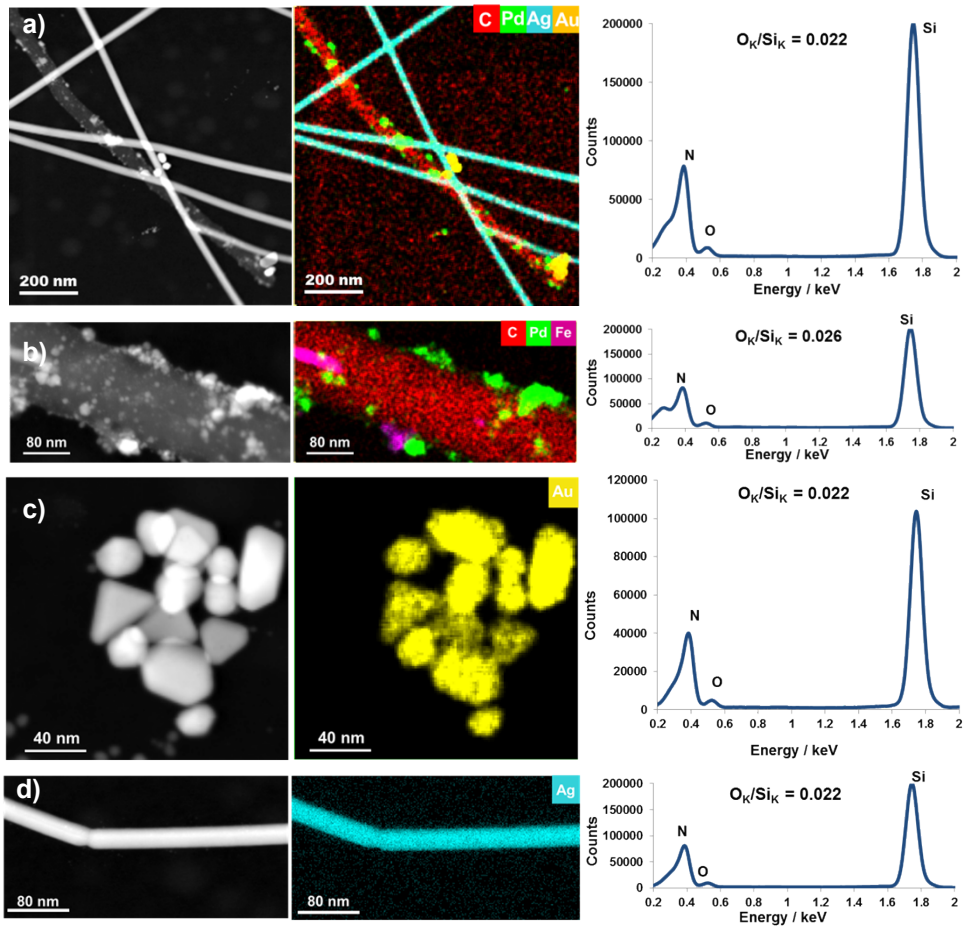

Fig. S1. a) Shows a region where all three components of the "soup" are present, b) shows a region of Palladium-decorated carbon nanotubes (Pd-CNT), c) shows a cluster of Gold nanoparticles (Au-NP), and d) shows a Silver nanowire (Ag-NW). In each case, the HAADF STEM image (left column), the spectrum image (middle column), and the 0-2 keV region of the XEDS spectrum are shown. Note the presence of iron in (b), this is the Fe catalyst left over from the CNT synthesis. The O_k/Si_k ratio for a dry sample is found, based on a total of 8 spectra, to be 0.024 ± 0.005.

S2. XEDS of wet samples

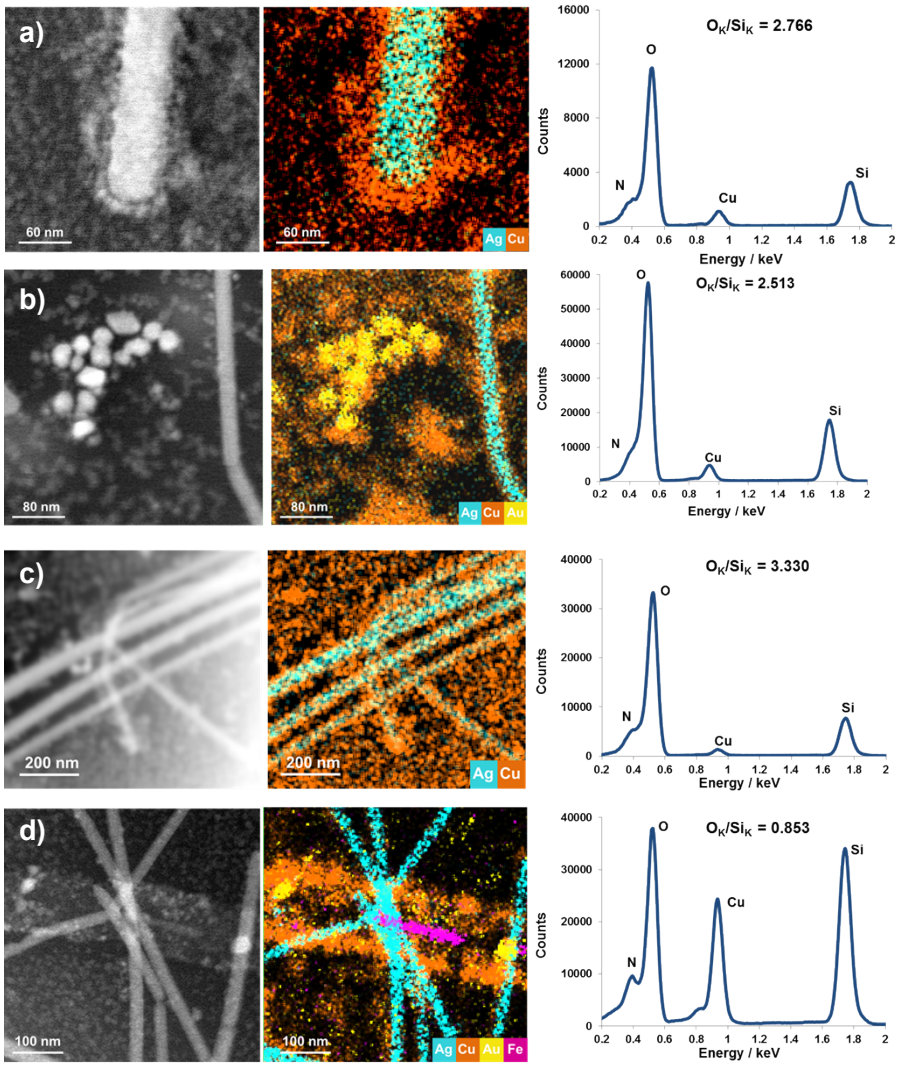

Fig. S2. A selection of spectrum images acquired from liquid-filled region of the e-cell. a) and d) are analysed in more detail in Fig.s 2 and 4. In each case, the HAADF STEM image (left column), the spectrum image (middle column), and the 0-2 keV region of the XEDS spectrum are shown. Comparing these XEDS spectra to those in Fig. S1, a dramatic change in the O_k/Si_k ratio is seen. The larger oxygen signal in these wet samples arises from the presence of water. While O_k/Si_k is almost constant for the dry references, here there is large variation form map-to-map, suggesting the amount of liquid present varies across the e-cell. This is consistent with the "tidal waves" observed during imaging (Video S7). In all spectrum images from liquid-filled regions of the e-cell, significant beam-induced Cu nanoparticle growth is observed.

S3. Growth rate quantification

A region of the image sequence shown in Figure 3 and Video S6 was analysed to estimate the areal growth rate of copper. Analysis was performed using ImageJ software, every 5th image of the sequence (equating to every 2.62s) was analysed. A threshold was applied to the HAADF images in the region of interest and used to determine the total nanoparticle area (Fig. S3). The region of interest was selected to contain a minimum of pre-synthesised nanostructures. Some growth occurred prior to beginning the data series and the area present at t=0 was therefore subtracted from all images. The resulting growth data shows two distinct regimes (Fig. 3d) with a higher initial rate between t=0 and t=15 and a lower, constant, rate of ≈550 nm^2s^{-1} for t>15 s.

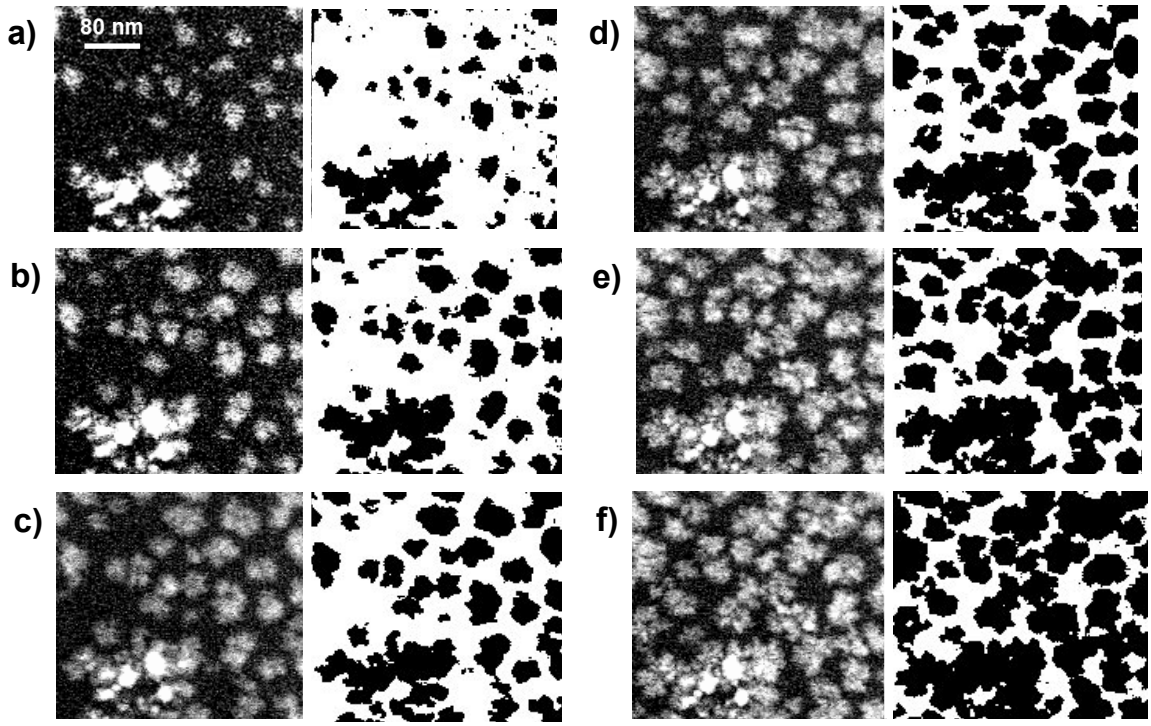

Fig. S3. HAADF STEM images were processed using ImageJ software to determine the rate of beam induced copper growth (Fig. 3 and Video S6). A threshold was applied to every 5th image to calculate the area of copper particles in the region of interest. Selected frames and the corresponding thresholded images are shown for times: t=8.4 s (a), t=24.10 s (b), t=39.83 s (c), t=55.54 s (d), t=68.64 s (e), and t=84.36 s (f). The resulting data (Fig. 3) shows a higher initial growth rate which decreases to a roughly constant rate of ≈550 nm^2s^{-1} after t=15 s.

S4. EELS thickness determination

Electron energy loss spectroscopy (EELS) is commonly used to estimate the thickness of TEM specimens.[1] t/λ values have previously been used in e-cell studies to determine liquid thickness and map the variable thickness arising from the bulging of the SiN_x windows.[2, 3]

As additional proof of the presence of liquid in our e-cells, EELS spectra were acquired from liquid-filled and liquid-depleted regions of the e-cell (Fig.s S4a and S4b respectively). These spectra show dramatically different t/λ values. Inelastic mean free paths for a variable thickness of water sandwiched between two 50 nm Si_3N_4 windows were calculated using Z_{eff} calculations (equations 1 and 2) as used by Jungjohann et. al.[1, 2] The liquid was approximated as H_2O and the windows assumed to be stoichiometric Si_3N_4. These calculations give an estimated liquid thickness of ≈180 nm in the liquid-filled region and ≈0 nm in the liquid-depleted region. Considering the 150 nm spacers employed and the extent of window bowing reported in the literature these results are consistent with our expectations of the e-cells geometry.

Equation 1:

$$Z_{eff} = \frac{\sum f_n Z_n^{1.3}}{\sum f_n Z_n^{0.3}}$$

Equation 2:

$$\lambda = \frac{106FE_0}{E_M ln(\frac{2\beta E_0}{E_M})}$$

Where:

$$E_M = 7.6Z_{eff}^{0.36}$$

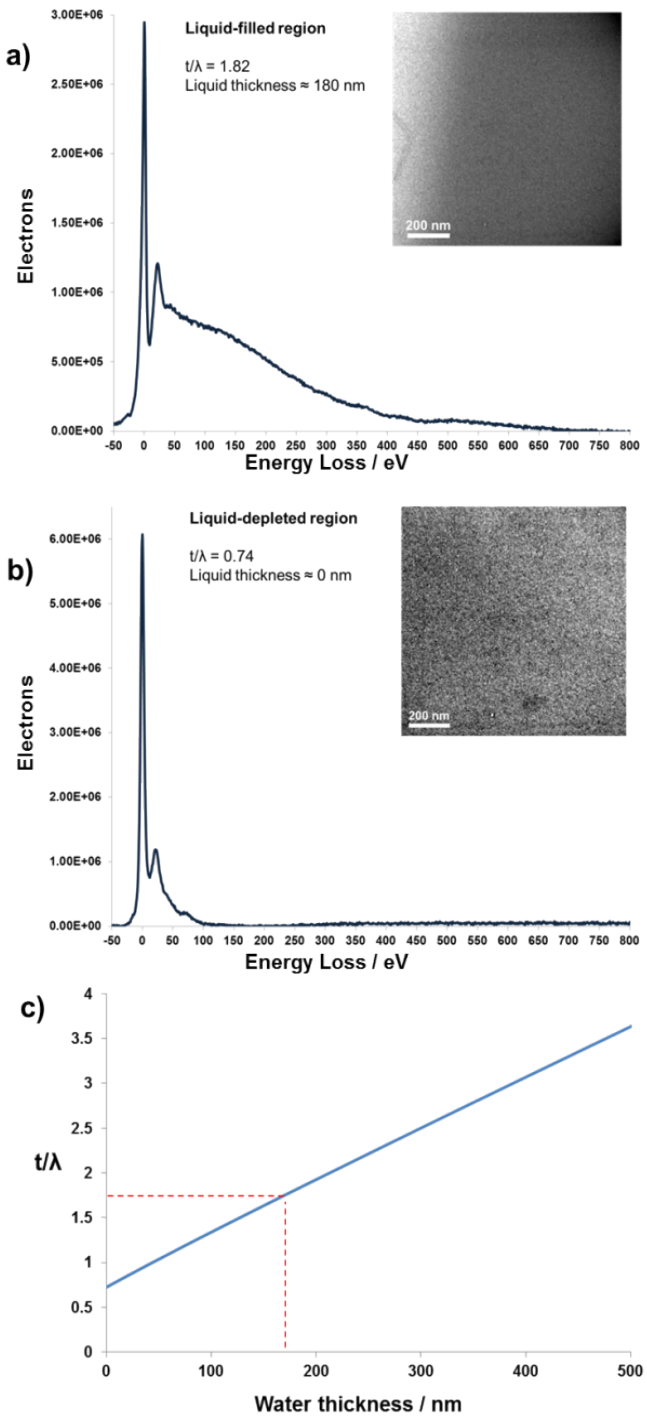

Fig. S4. EELS spectra from a liquid-filled (a) and liquid-depleted (b) region of the e-cell were acquired and their t/λ values calculated. Inelastic mean free path (λ) values based of Z_{eff} calculations were found for e-cells containing different thicknesses of water (c) and used to estimate the thickness of the liquid layers in the two regions. Estimated liquid thicknesses of 180 nm and 0 nm were calculated for the liquid-filled and the liquid-depleted regions respectively.

S5. Tilt and position dependence of X-ray counts

Despite its dramatic reduction due to the modified holder design, experimental set-up is still important to minimize X-ray shadowing. X-ray counts can be maximised through choice of holder tilt and the region of the e-cell studied. Figure S5 demonstrates that for high α tilt angles, significant X-ray signal is obtained over a large area of the 400 x 50 µm window of the e-cell. In this work (spectrum images shown in Fig.s 2, 4 and S2) an α tilt angle of 30° was employed and shadowed regions of the e-cell were avoided to maximise the efficiency of spectral data collection.

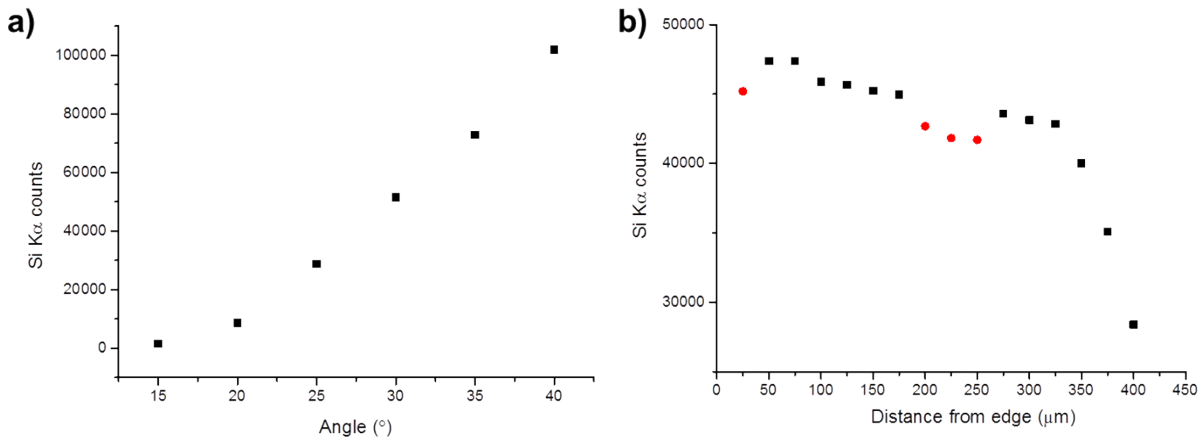

Fig. S5. A strong X-ray signal is observed for a wide range of positions. a) Si K-edge signal as a function of holder tilt angle for a central point in the window demonstrating that greater shadowing occurs at low tilt angles. b) Si K – edge signal as a function of position along the window long axis (perpendicular to the axis of the in-situ specimen holder) demonstrating that a wide range of positions allow viable spectral data collection The data points in red for (b) were taken from regions where due to breaks in one of the windows only a single 50 nm SiN_x window was present instead of the two windows that were present for the other (black) data points. To correct for this the Si_K - counts from single window regions have been doubled.

S6. Video: Beam induced copper growth

This video shows the growth of copper nanoparticles in the presence of other pre-synthesised nanostrucutures (Au-NWs and Pd-CNTs). This process is beam-induced; with electrons from the imaging probe reducing copper ions from the aqueous solution. Quantitative analysis of this video allowed the areal growth rate to be estimated (Fig.s 3 and S3).

S7. Video: Movement of liquid

The e-cell is incompletely filled with the aqueous nanoparticle "soup" solution. The e-cell contains air pockets, at atmospheric pressure, resulting in liquid-filled and liquid-depleted regions (Fig.s 1 and S4). The liquid-depleted regions are transient in nature, with liquid moving around the cell. Due to the presence of the air pockets, liquid can be manipulated to flow into different regions of the e-cell. This video (Video S7) shows the movement of a liquid wavefront during imaging. The flow of liquid results in the displacement of nanostructures, which are transported as the transient wave front moves across the field of view, relocating the entrapped atmospheric pocket. Such "nanoscale tidal waves" have been reported in previous e-cell studies.[4]

References

1 R. F. Egerton, *Electron Energy-Loss Spectroscopy in the Electron Microscope*, Springer Science, New York, 2011.

2 K. L. Jungjohann, J. E. Evans, J. A. Aguiar, I. Arslan and N. D. Browning, *Microscopy and Microanalysis*, 2012, **18**, 621.

3 M. E. Holtz, Y. Yu, J. Gao, H. D. Abruna and D. A. Muller, *Microscopy and Microanalysis*, 2013, **19**, 1027.

4 M. J. Dukes, B. W. Jacobs, D. G. Morgan, H. Hegde and D. F. Kelly, *Chemical Communications*, 2013, **49**, 3007.